Appendix B8

Finite Element Analysis

Seismic Analysis of a Section of Watana Dam

1. Introduction

This document reports the findings of the effect of using LS-DYNA to analyze a simple 2D model of the proposed cross section of the Watana Dam and to demonstrate that inclusion of a massed foundation and representation of the reservoir as a compressible material has a beneficial result on stresses (compared to the massless analysis). The analysis included simulations of the dam-foundation-reservoir response to the GIL earthquake record and the results are presented herein.

A cross-section of the tallest monolith of the dam has been modelled along with a section of the reservoir and foundation. Two simulations have been are performed, the first used the Ansys-Mechanical software while LS-DYNA was used for the second simulation.

The Ansys-Mechanical model had massless foundation and hydrodynamic effects were included using the Westergaard approach. Additionally the Ansys-Mechanical solver uses implicit method of time integration through the seismic event.

LS-DYNA uses an explicit method of time integration for time history analysis. The model analyzed also had massed foundation and the reservoir was represented as a compressible fluid. As a result, non-reflecting boundaries were assigned to the cut edges of the foundation and reservoir. The seismic excitations were implemented as tractions at the bottom edge of the foundation and were subsequently scaled to produce the correct outcrop accelerations.

Table 1 presents a comparison of the different concepts used in the two simulations.

Table 1 - Comparison of the Concepts in the Two Solutions

Software	Solver	Foundation Concept	Hydrostatic Pressure	Hydrodynamic Concept	Seismic Excitation	Non-reflecting Boundaries
Ansys-Mechanical	Implicit	Massless	Direct Pressure	Westergaard Mass	Velocity	N/A
LS-DYNA	Explicit	Massed	Reservoir Self-Weight	Compressible Reservoir	Traction	Foundation and Reservoir

The results of these simulations are contained in this report and clearly demonstrate that the stresses and sliding displacements reduce substantially when massed foundation and compressible reservoir concepts are implemented in simulations.

2. Geometry and FEA Mesh

The geometry and mesh used in the simulations are presented in Figure 1 and Figure 2. The models were similar for both explicit and implicit simulations.

For the implicit (Ansys-Mechanical) simulation, the reservoir was replaced with an equivalent hydrostatic pressure and Westergaard masses on the dam's upstream face. The density of foundation was reduced to a small fraction in order to model according to massless concept.

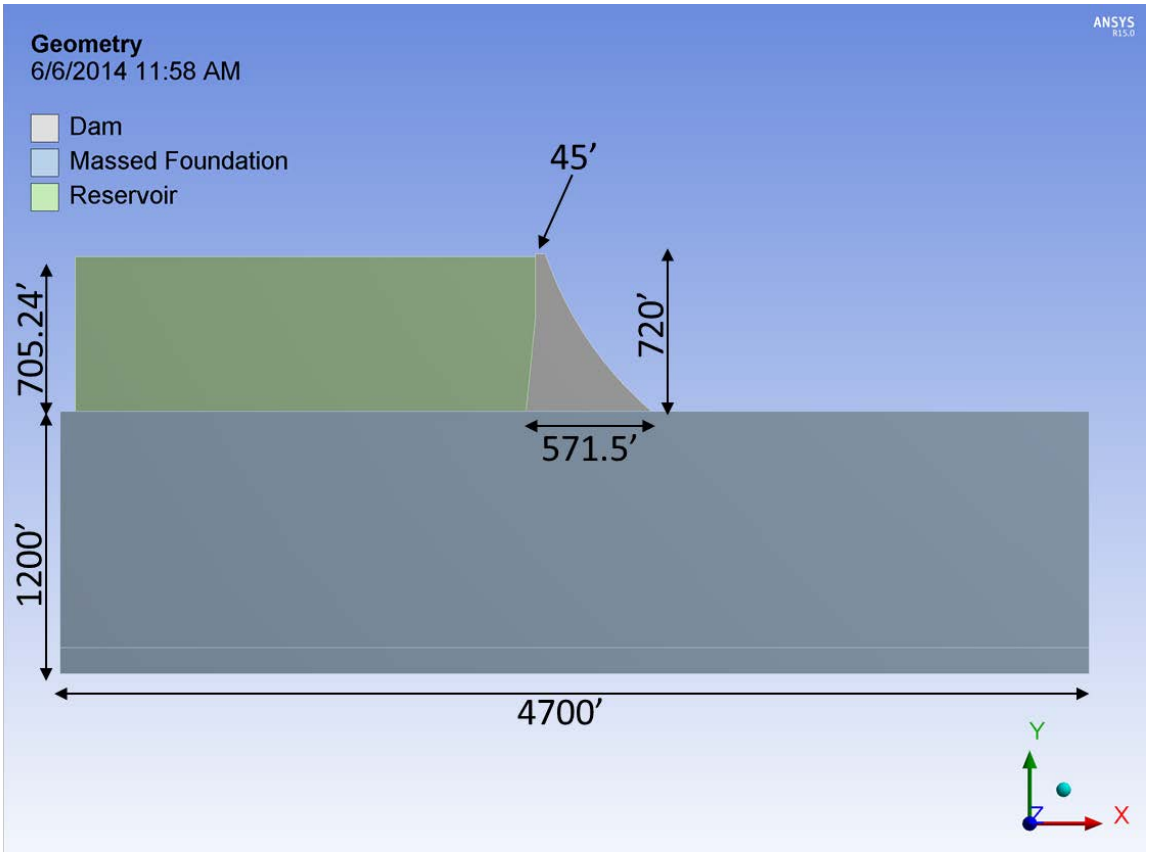

Figure 1 – Geometry and materials in explicit simulation. There is no reservoir body and the foundation is massless in implicit simulation

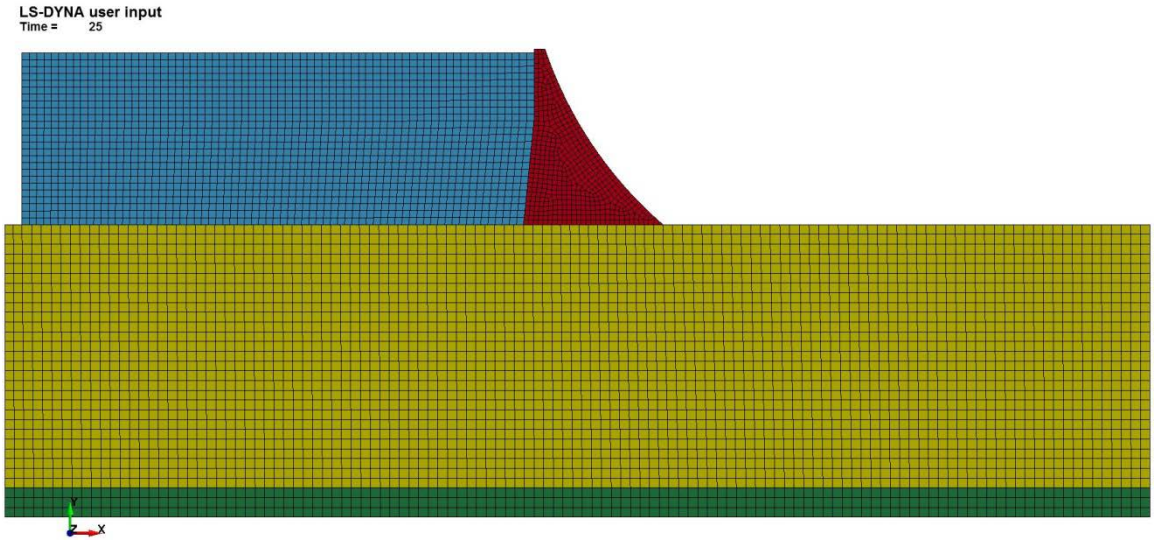

Figure 2 – FEA Mesh in explicit simulation. Reservoir mesh is removed in implicit simulation

3. Material Properties

3.1. Dam Concrete

Table 2 summarizes the material properties used for dam concrete in the simulations.

Table 2 – Dam Concrete Material Properties

Mass Density	Deformation Modulus	Poisson's Ratio
ρ (pcf)	E (psi)	v
150	4E+06	0.25

3.2. Foundation Rock

The foundation material properties used in the simulations are shown in Table 3.

Table 3 – Foundation Rock Material Properties

Mass Density	Deformation Modulus	Poisson's Ratio
ρ (pcf)	E (psi)	v
170	3.5E+06	0.25

3.3. Reservoir Water

The reservoir water properties used in the explicit model simulation is stated in Table 4. Bulk modulus was included using an equation of state. These properties only applied to the LS-DYNA model.

Table 4 – Reservoir Water Material Properties

Mass Density	Bulk Modulus
ρ (pcf)	K (psi)
62.4	3.1E+05

4. Compressible Reservoir and Massed Foundation Boundary Conditions

The explicit simulation required the removal of the displacement supports from the far end of the reservoir and foundation (the cut faces) and replaced with a non-reflecting boundary condition for the seismic analysis.

4.1. Removal of Displacement Supports

Initially a quasi-static analysis was performed to determine the support reactions at the cut boundaries of the foundation and reservoir. This involved adding roller supports to these boundaries as indicated in Figure 3 and a simulation was performed within LS-DYNA. The gravity loads of the dam and reservoir were ramped up in 5 seconds of analysis and the analysis was continued for another 5 seconds in order that the system reached the at rest condition. The selected system damping ratio was 7 times the transient damping ratio in order to ensure reaching at rest condition.

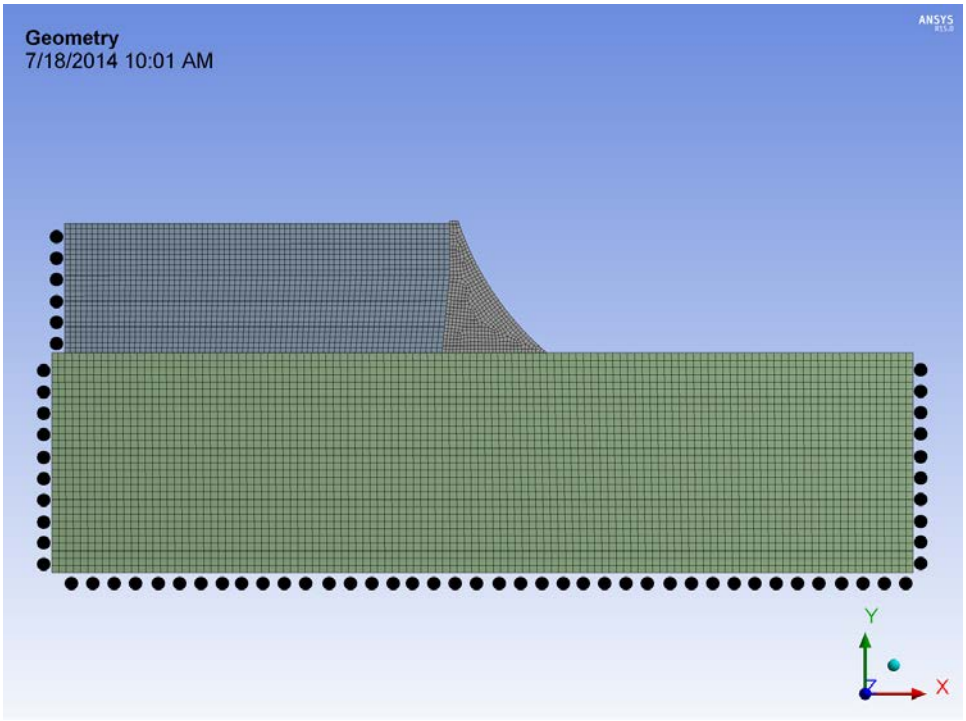

Figure 3 – Schematics of support condition for quasi-static analysis

To perform the transient analysis with a massed foundation, the displacement supports were removed and replaced by their corresponding nodal forces calculated by the quasi-static simulation. The intention of this procedure was to prevent reflection of seismic waves at the displacement boundaries.

4.2. Non-Reflecting Boundaries

Non-reflecting boundary conditions were implemented at the cut faces of the reservoir and foundation to absorb the outgoing waves to prevent their reflection within the system.

5. Dam – Foundation Interface

Frictional contact was used at the dam-foundation interface both in explicit and implicit simulations. This interface does not transfer tensile stresses but compressive stress is transferred while shear stress transfer is limited to the product of the frictional coefficient and compression stress.

Both static and dynamic coefficients of friction were set to

$$\mu_s = \mu_d = 1.2$$

For modal analysis this contact was changed to bonded type.

6. Modal Analysis

A modal analysis of the system was performed to give an indication of system behavior and the healthiness of modeling concepts. The estimated major mode shapes and frequencies were used in determining the Rayleigh damping factors and upper limits of the mesh size and time increment. A realistic estimate of the main frequency of the system is also important for seismologists and geotechnical engineers to determine the design spectral response and seismic excitations.

Modal analysis was performed on the model with the same finite element mesh. The contact between the dam and foundation was changed to bonded type and the foundation was considered to be massless. The cut faces of the foundation had frictionless supports to prevent displacements that would normal to them.

Models with and without hydrodynamic effects are presented herein to show the importance of the reservoir contribution to seismic response. Two sets of results using the Westergaard incompressible concept and the results from the compressible concept (acoustic) are presented.

6.1. Model without Reservoir

A modal analysis was performed on a model with no reservoir. Three main modal frequencies and their corresponding modal mass ratios in both directions are presented in Table 5 along with the cumulative ratios. Figure 4 shows the directional deformations in X-direction for mode 1. Table 5 shows that modes

1 and 2 are mainly horizontal while mode 3 is vertical. It also shows that more than 90% of the mass is achieved by mode 3.

Table 5 – Major Modes of System Resulted from the Modal Analysis without Reservoir

Mode	Frequency	Period	Ratio of Effective Mass to Total Mass			
	f (Hz)	T (sec)	X-Direction individual	X-Direction Cumulative	Y-Direction individual	Y-Direction Cumulative
1	1.4667	0.6818	0.5618	0.5618	0.0200	0.0200
2	3.0416	0.3288	0.3549	0.9167	0.0682	0.0883
3	3.239	0.3087	0.0005	0.9172	0.8682	0.9565

6.2. Model with Westergaard Mass

Modal analysis was repeated on a model where reservoir hydrodynamic effect was implemented by Westergaard nodal masses. Three main modal frequencies and their corresponding modal mass ratios are presented in Table 6. Table 6 shows that modes 1 and 2 are majorly horizontal and mode 3 is vertical. It also shows more than 90% of the mass is achieved by mode 3.

Table 6 – Major Modes of System Resulted from the Modal Analysis with Westergaard Masses

Mode	Frequency	Period	Ratio of Effective Mass to Total Mass			
	f (Hz)	T (sec)	X-Direction individual	X-Direction Cumulative	Y-Direction individual	Y-Direction Cumulative
1	1.0836	0.9228	0.5994	0.5994	0.0086	0.0086
2	2.3795	0.4203	0.3148	0.9143	0.0006	0.0092
3	3.2035	0.3122	0.0096	0.9238	0.9390	0.9483

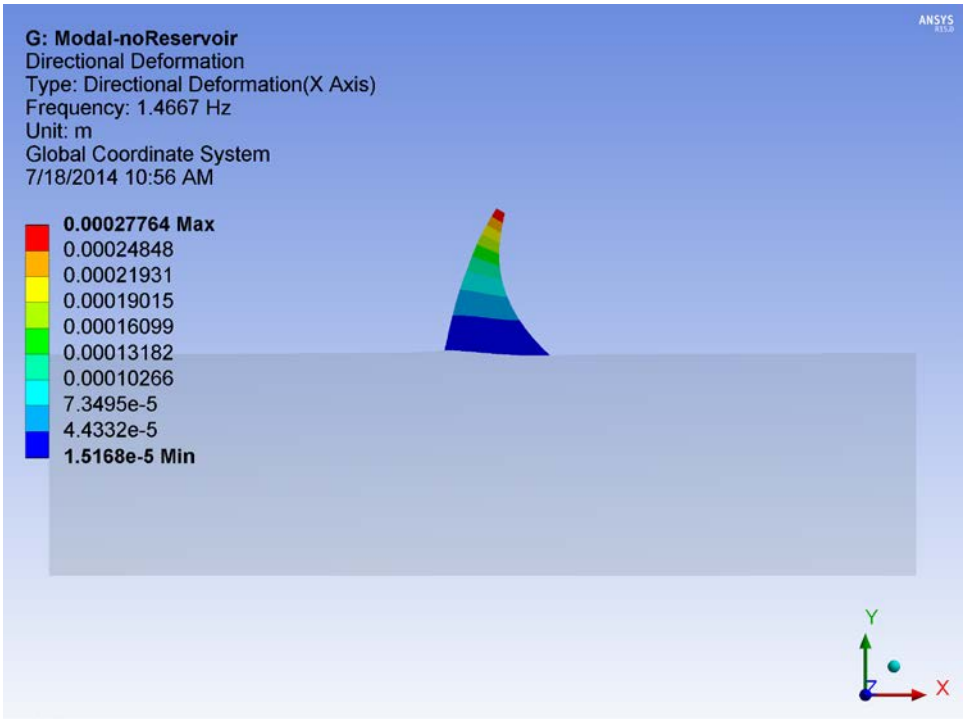

Figure 4 – First mode shape of the system resulted from the modal analysis without Reservoir

6.3. Model with Compressible Representation of Reservoir

A third modal analysis was performed on a model where reservoir is represented by an acoustic body. Three main modal frequencies and their corresponding modal mass ratios in both directions are presented in Table 7. This analysis resulted in the most accurate estimation of the first mode of vibration of the system. Modal mass ratios from this analysis could be misleading as they were obtained using the whole mass of reservoir.

Table 7 – Major Modes of System Resulted from the Modal Analysis with Compressible Representation of Reservoir

Mode	Frequency	Period
	f (Hz)	T (sec)
1	1.1403	0.8770
2	1.5683	0.6376
3	1.9242	0.5197

7. Transient Analysis Settings

7.1. Rayleigh Damping

Massless Foundation Concept

A global damping ratio of $\xi = 7\%$ was used for implicit simulation in Ansys-Mechanical and Rayleigh damping factors were calculated based on the following equations:

$$\alpha = 2\xi\omega_1 \frac{2R}{1+R+2\sqrt{R}}, \qquad \beta = 2\xi \frac{1}{\omega_1} \frac{2}{1+R+2\sqrt{R}}$$

The main circular frequency of $\omega_1 = 6.81\, rad/sec$ $(f_1 = 1.08\, Hz)$ and $R \cong 3.0$ was used. The equations determined a mass coefficient of $\alpha = 0.762/sec$ and a stiffness coefficient of $\beta = 5.56E-3\ sec$. The variation of Rayleigh damping with period is presented in Figure 5.

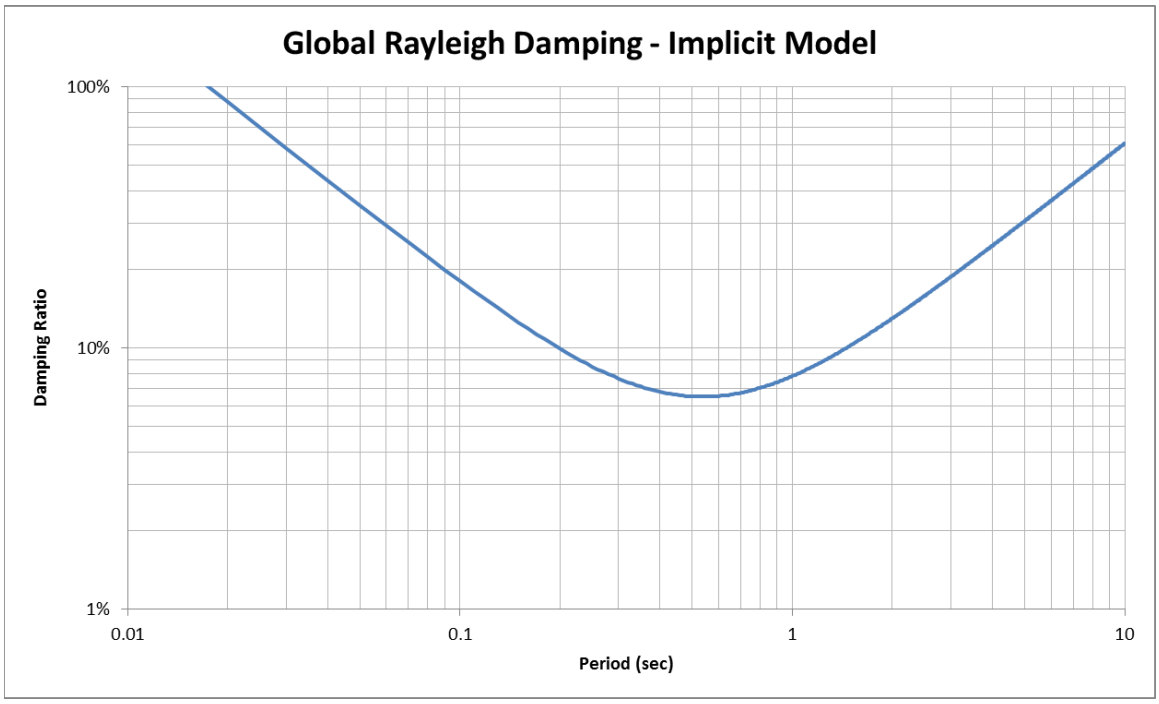

Figure 5 – Rayleigh Damping Diagram for $\alpha = 0.762/sec$ and $\beta = 5.56E-3\ sec$

Massed Foundation Concept

Rayleigh mass coefficient of $\alpha = 0.4/sec$ was used for explicit simulations in LS-DYNA and the stiffness coefficient was set to zero. Variation of damping ratio with frequency in this case is presented in Figure 6.

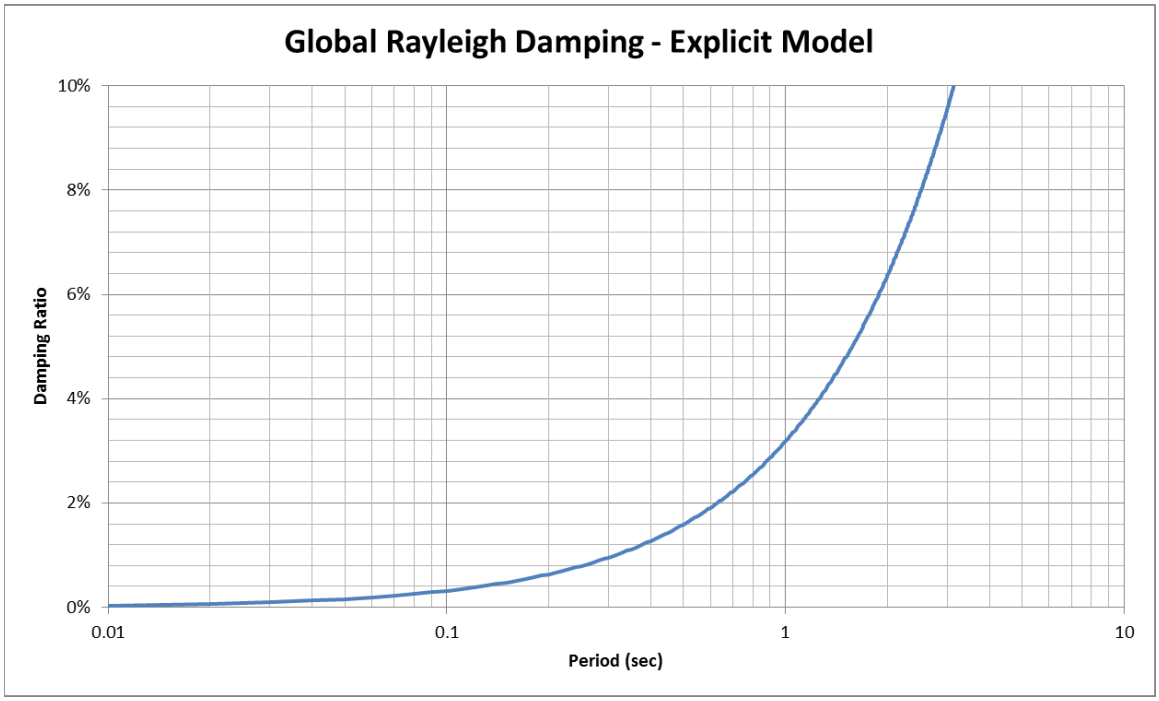

Figure 6 – Rayleigh Damping Diagram for $\alpha = 0.4/sec$ and $\beta = 0.0\ sec$

7.2. Element Sizes in Simulations

The element sizes used in the model are presented in Table 8. The shear wave velocity in the foundation ($V_s \cong 6000\ ft/sec$), generates frequencies as high as 15 Hz which are accommodated with an element size of 40' resulting in minimum 10 elements per wavelength.

Table 8 – Element Size in Model Bodies

	Dam	Foundation	Reservoir
Element Size	20'	40'	30'

7.3. Time Increments

The time increment was determined using the equation below. The increment was selected to ensure frequencies as high as 15 Hz could be accommodated. The maximum allowable time increment would be:

$$\delta t_{MAX} \leq \frac{1}{8 \times 15} \cong 0.008\ sec$$

The selected maximum time increment was set to 0.005 sec in the implicit simulation while the minimum time increment was 0.00001 sec.

LS-DYNA automatically calculates the time increment necessary for a stable explicit solution. The program was set to use 20% of its calculated value and as a result a constant time increment equal to 0.00013 sec was used throughout the explicit simulation.

8. Loading

8.1. Dam Weight

Dam weight was modeled in both simulations. The gravitational acceleration used in the simulations was:

$$g = 32.18\ ft/sec^2$$

8.2. Reservoir Weight / Hydrostatic Pressure

The weight of the reservoir was implemented in the explicit simulation with the gravitational acceleration as stated above. For the implicit simulation, reservoir pressure was applied to dam – reservoir interface as

$$P_{hydrostatic} = \frac{(62.4 \times h)}{12^2}$$

Where:

- h(ft)is the depth of an interface point in the reservoir and
- $P_{hydrostatic}\ (psi)$ is its hydrostatic pressure.

8.3. Hydrodynamic Pressure

In the explicit simulation, seismic pressure waves were produced in the compressible reservoir and resulted in hydrodynamic pressure on the dam. In the implicit simulation, hydrodynamic pressures were simulated using Westergaard masses added to the dam upstream face.

8.4. Seismic Loading

GIL Earthquake record as shown in Figure 7 was used as the base excitation in the simulations.

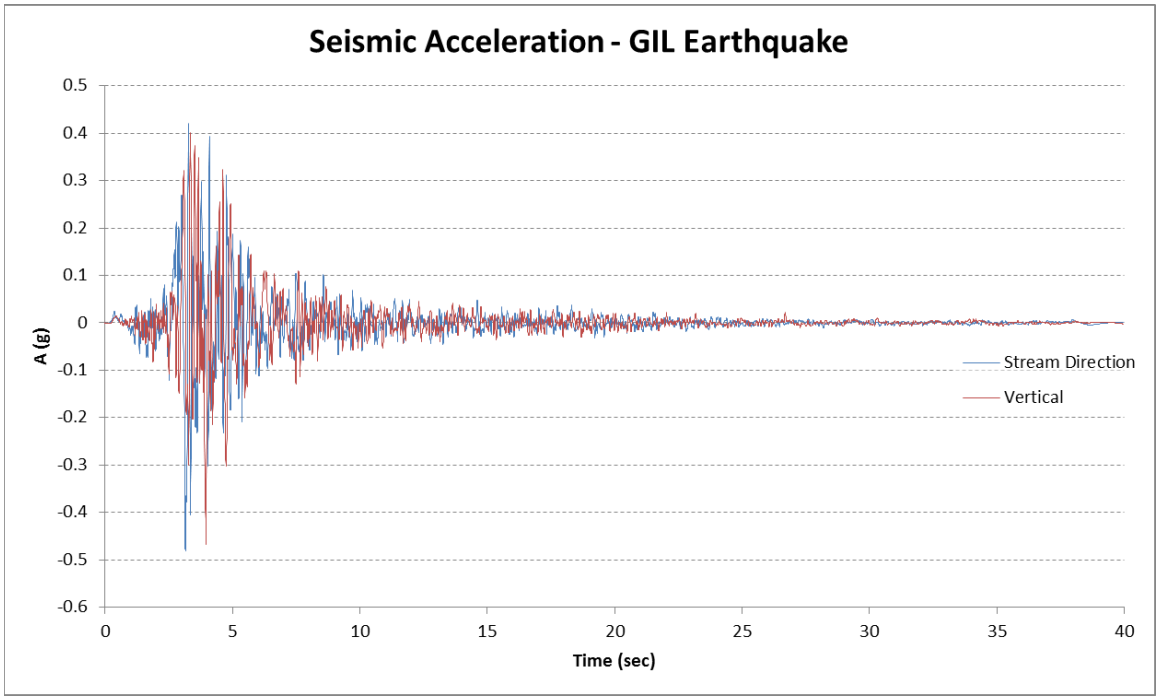

Figure 7 – Stream-Direction and Vertical Components of GIL Seismic Record (acceleration)

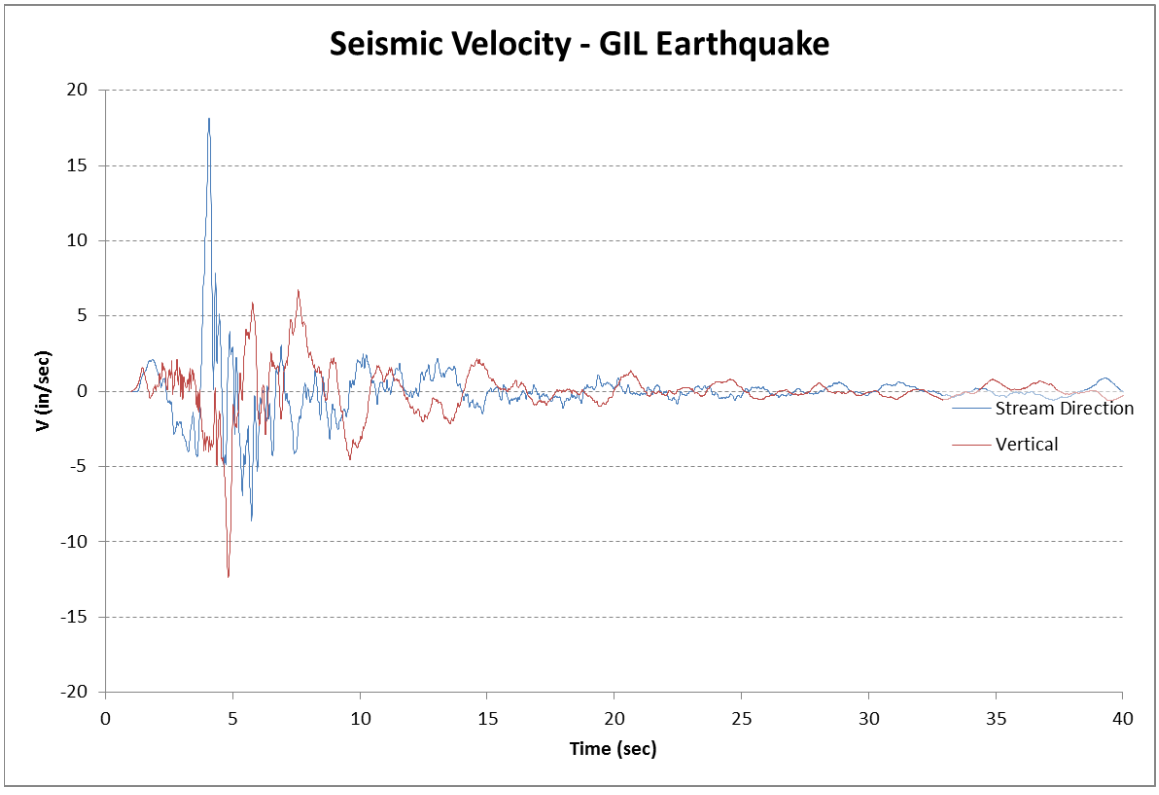

Figure 8 – Stream-Direction and Vertical Components of GIL Seismic Record (velocity)

In the implicit simulation with a massless foundation, the seismic velocity (Figure 8) was used as input on the base and sides of the foundation and in the simulation. The explicit massed foundation analysis, seismic excitation was applied as traction records to avoid seismic wave reflection. A deconvolution analysis determined the damper coefficients used in calculating these tractions which were applied close to the base (at the interface of the red and blue zones of the foundation as colored in Figure 9).

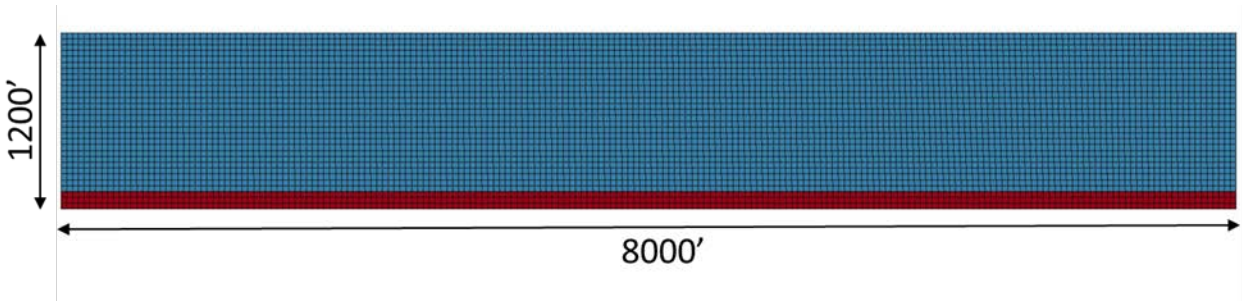

Figure 9 – Foundation Model in De-convolution Analysis

9. De-convolution Analysis

The de-convolution analysis was performed to determine damper coefficients from the seismic velocities which were used in calculating the seismic tractions that were subsequently applied to the massed foundation. Lysmer dampers were used as the initial damper coefficients which were updated by the de-convolution analysis. The analysis ensured that the final coefficients accounted for the actual foundation geometry and mesh. The following table summarizes the Lysmer damper values for the foundation.

Table 9 – Foundation Rock Wave Velocities and Lysmer Damper Coefficients

Shear Wave Velocity	Longitudinal Wave Velocity	Lysmer Damper - Tangential	Lysmer Damper - Normal
V_S (ft/sec)	V_L (ft/sec)	c_t (psi.sec/in)	c_n (psi.sec/in)
6177.2	10698.8	18.89	32.71

In order to verify and update above damper coefficients, a model of foundation was prepared as shown in Figure 9 with similar geometry, mesh size and global damping ratio as in the section model and with absorbing boundary conditions implemented to its cut faces at the base and sides. The initial estimates of tractions were calculated as the product of Lysmer damper (tangential for shear directions and normal for vertical direction) and the corresponding velocities from Figure 8. These tractions were applied at an interface which is 3 element heights above the base of the foundation.

The de-convolution analysis involved the creation of a model of the foundation with similar geometry, mesh size and global damping ratio as in the cross section model. The cut faces at the base and sides of the foundation model were defined with absorbing boundary conditions. The foundation traction records

were initially calculated using Lysmer damper values (tangential for shear directions and normal for vertical direction) and the corresponding velocities from Figure 8. These tractions were applied at an interface within the foundation model which is 3 elements high as shown in red in Figure 9.

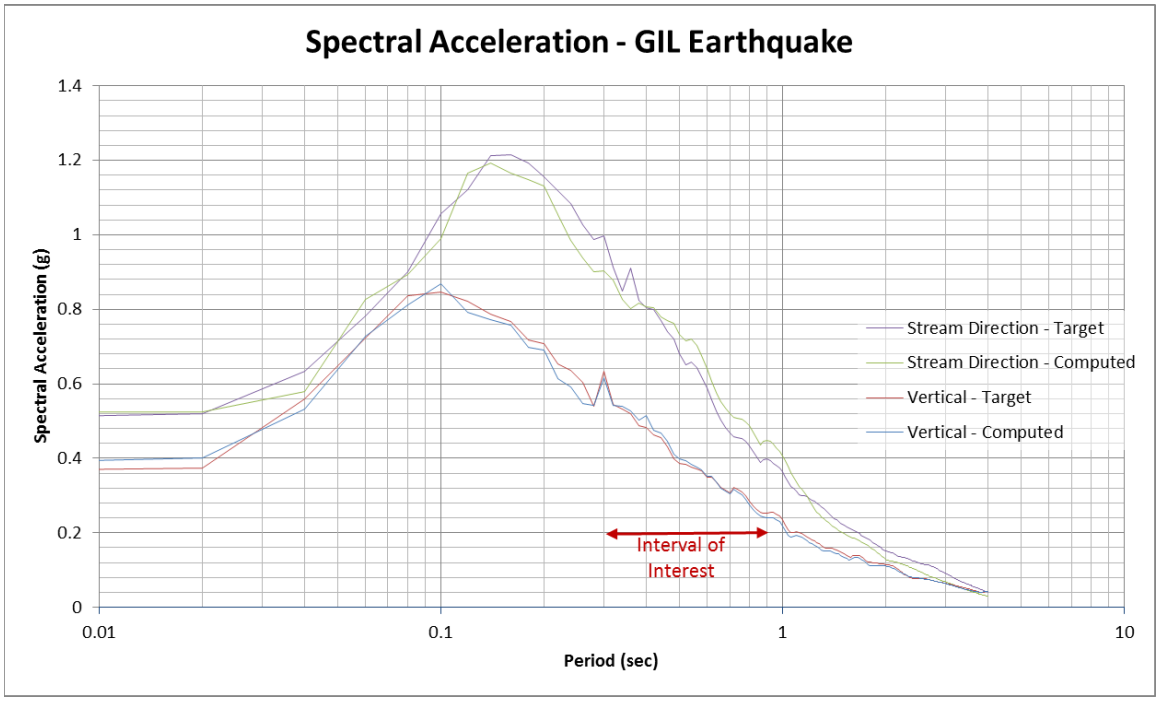

Figure 10 – Spectral Acceleration of the Target Seismic Record Compared with Spectral Acceleration of Computed Record

The foundation model described above was then analyzed and the resulting components of acceleration at the top of the foundation were recorded. The spectral acceleration responses were computed for these two components and then compared with the corresponding spectral responses of the free-field motions. The damping factors were adjusted so that the responses closely matched at the period range of interest. This procedure is presented in Figure 10.

The de-convolution procedure adjusted the values of damping coefficients to those shown in Table 10. These values were used in explicit (LS-DYNA) simulation.

Table 10 – Adjusted Damping Coefficients Resulted from De-convolution Analysis

Stream Direction	Vertical Direction
c_x (psi.sec/in)	c_y (psi.sec/in)
17.76	32.84

10. Static Analysis Results

Figure 11 shows the vertical stress distribution at the end of static analysis in Ansys-Mechanical and Figure 12 shows the vertical stress distribution at the end of quasi-static analysis in LS-DYNA. Figure 13 shows the hydrostatic pressure distribution in the reservoir at the end of quasi-static analysis. Quasi-static analysis procedure is described in Section 4.

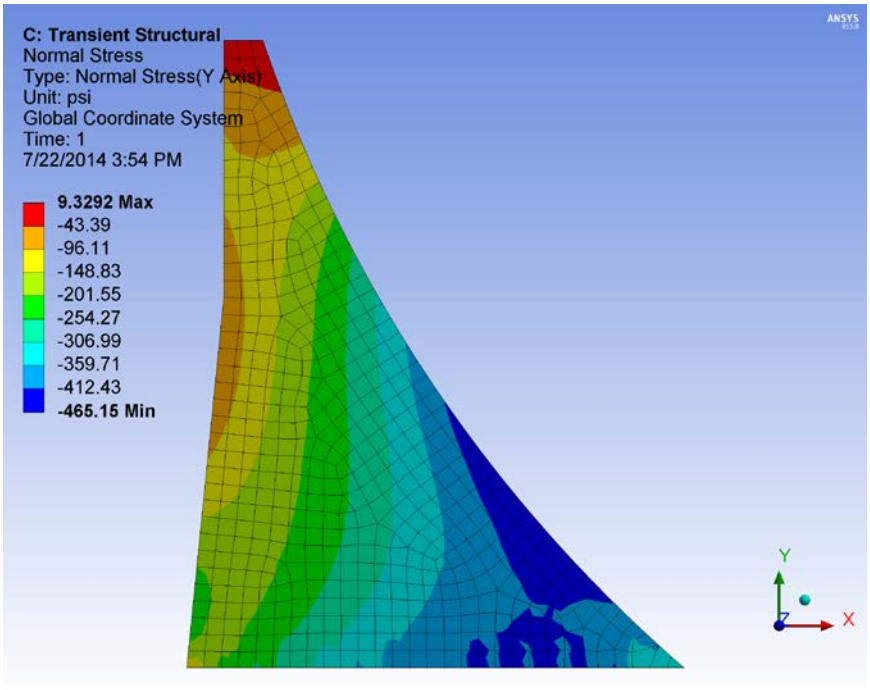

Figure 11 – Static Vertical Stress Distribution in Dam due to Weight and Hydrostatic Pressure (Ansys-Mechanical Model)

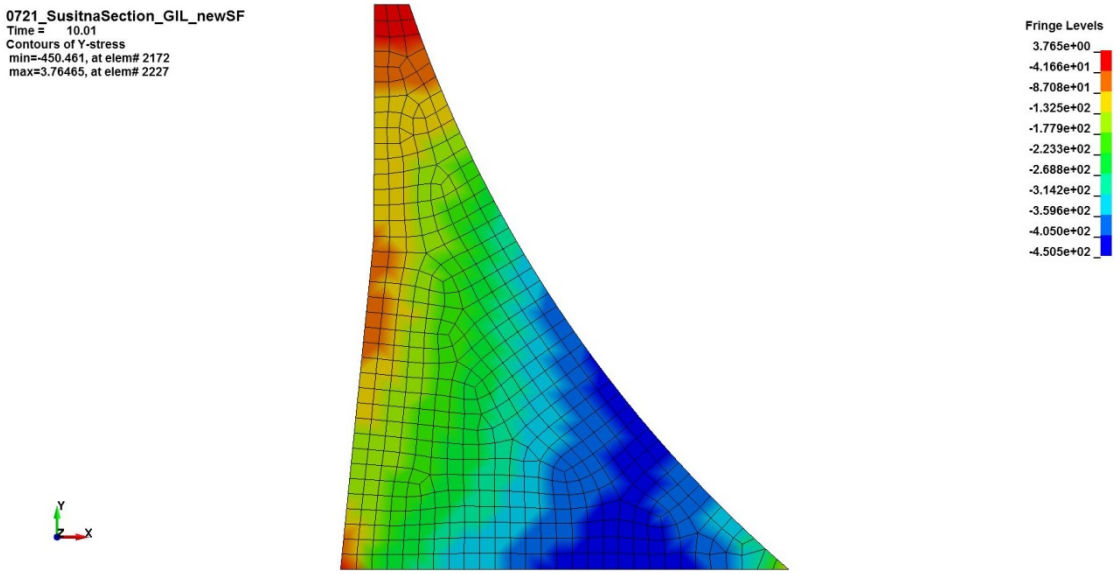

Figure 12 – Static Vertical Stress Distribution in Dam due to Weight of Dam and Reservoir (quasi-static analysis in LS-DYNA)

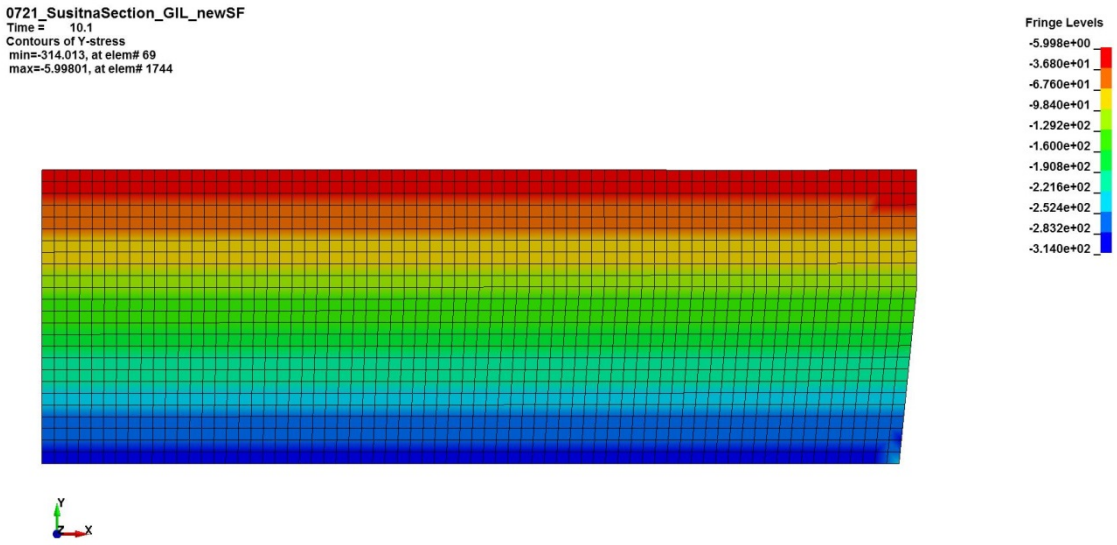

Figure 13 – Hydrostatic Pressure Distribution in Reservoir (quasi-static analysis in LS-DYNA)

11. Seismic Simulations

Dam stresses are presented for massless and massed foundation simulations. This is followed by comparative diagrams of monolith sliding, top of monolith displacement, monolith stresses and reservoir pressure.

11.1. Implicit Simulation with Westergaard Masses and Massless Foundation

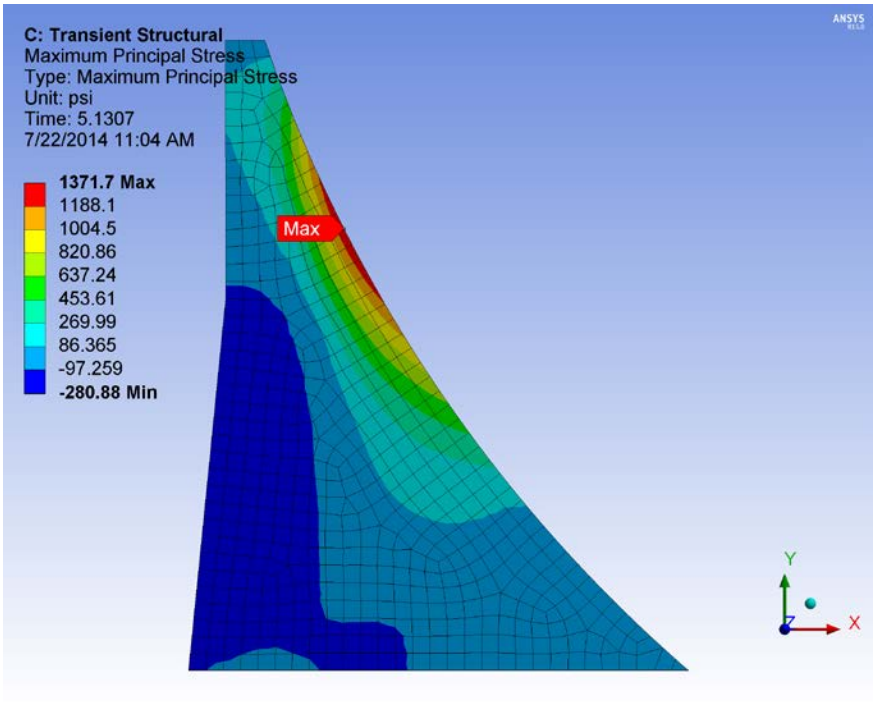

Figure 14 – 1st Principal Stress at the Moment when it is Maximum on D/S Face of Monolith

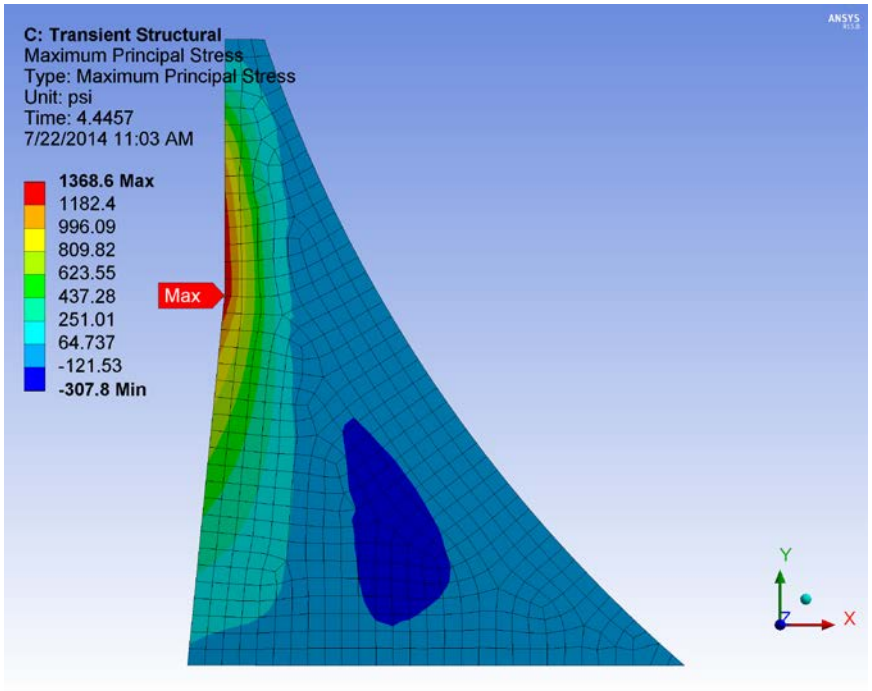

Figure 15 – 1st Principal Stress at the Moment when it is Maximum on U/S Face of Monolith

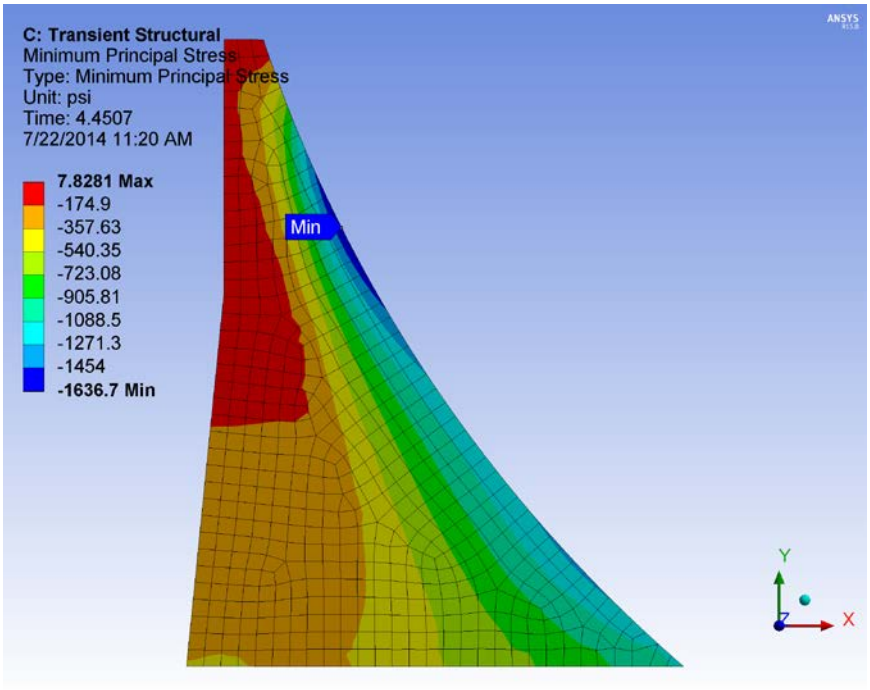

Figure 16 – 3rd Principal Stress at the Moment when it is Minimum on D/S Face of Monolith

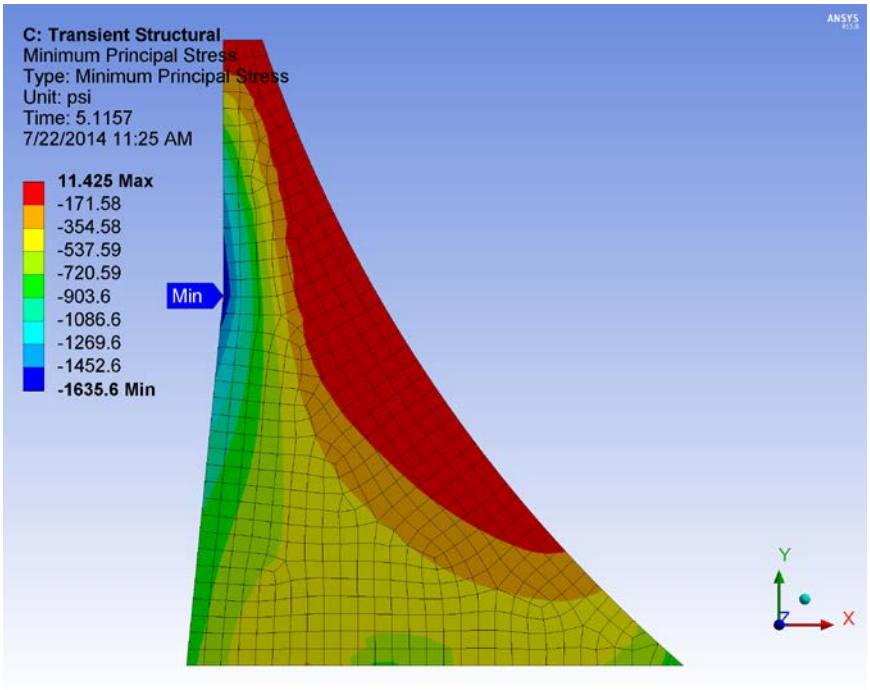

Figure 17 – 3rd Principal Stress at the Moment when it is Minimum on U/S Face of Monolith

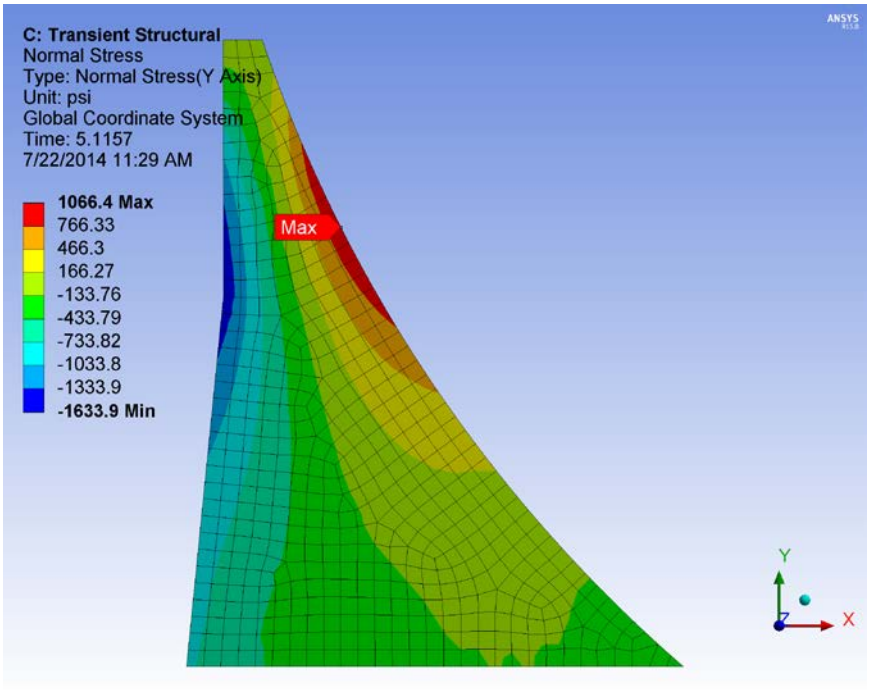

Figure 18 – Vertical Stress at the Moment when it is Maximum on D/S Face of Monolith

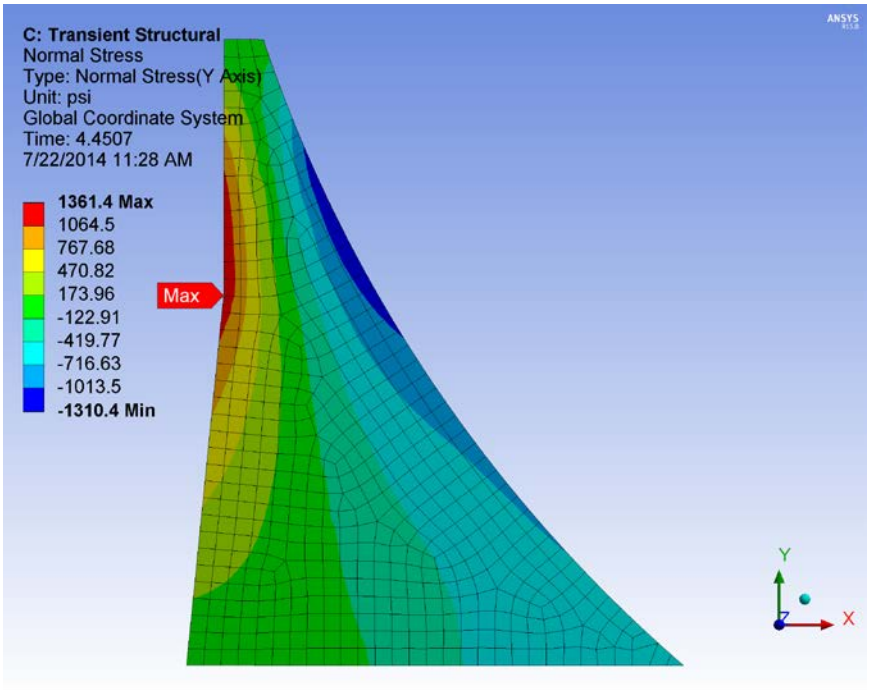

Figure 19 – Vertical Stress at the Moment when it is Maximum on U/S Face of Monolith

11.2. Explicit Simulation with Compressible Reservoir and Massed Foundation

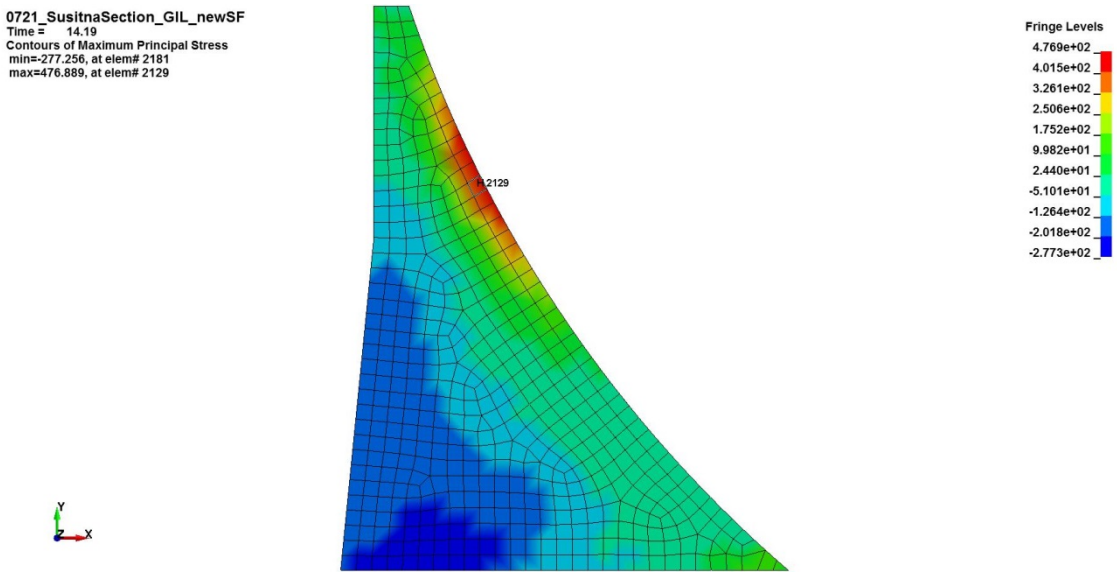

Figure 20 – 1st Principal Stress at the Moment when it is Maximum on D/S Face of Monolith

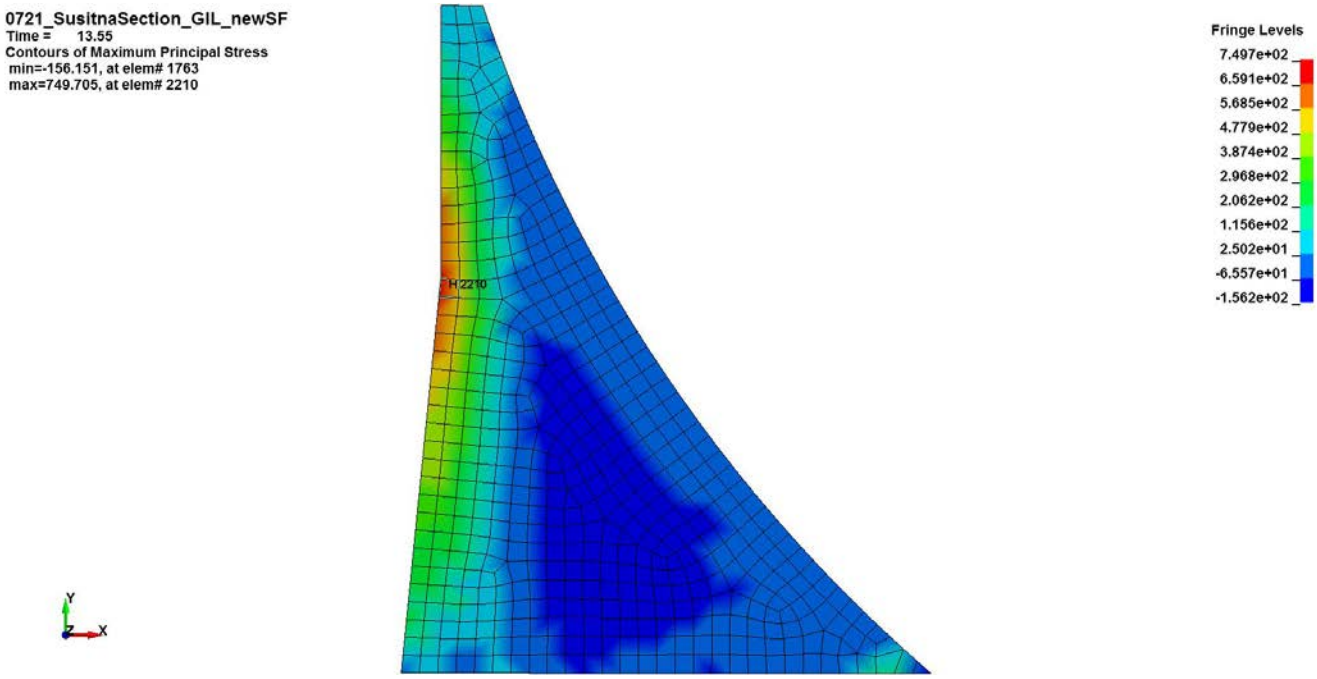

Figure 21 – 1st Principal Stress at the Moment when it is Maximum on U/S Face of Monolith

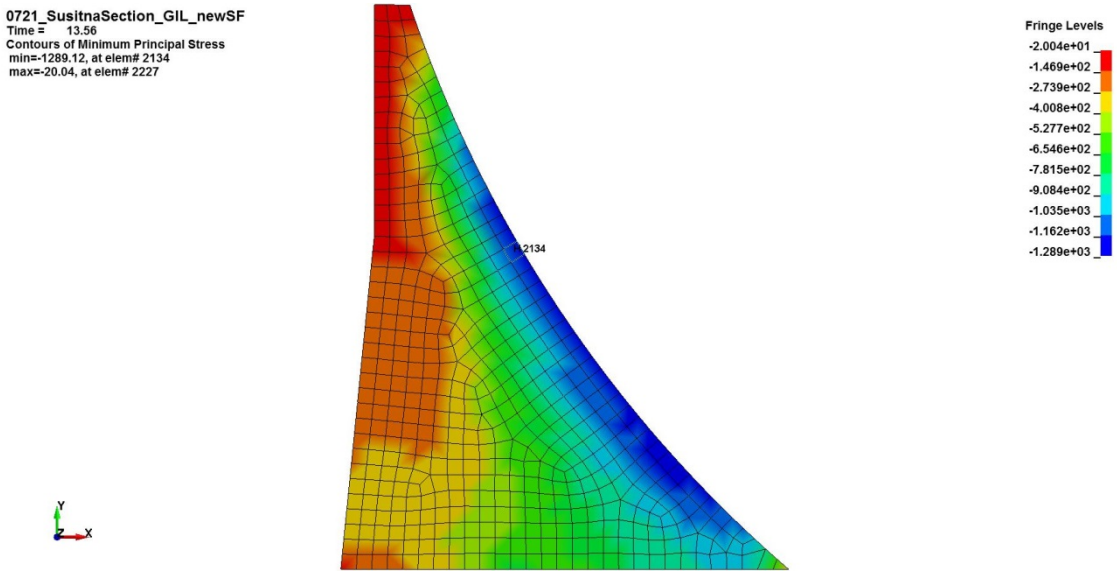

Figure 22 – 3rd Principal Stress at the Moment when it is Minimum on D/S Face of Monolith

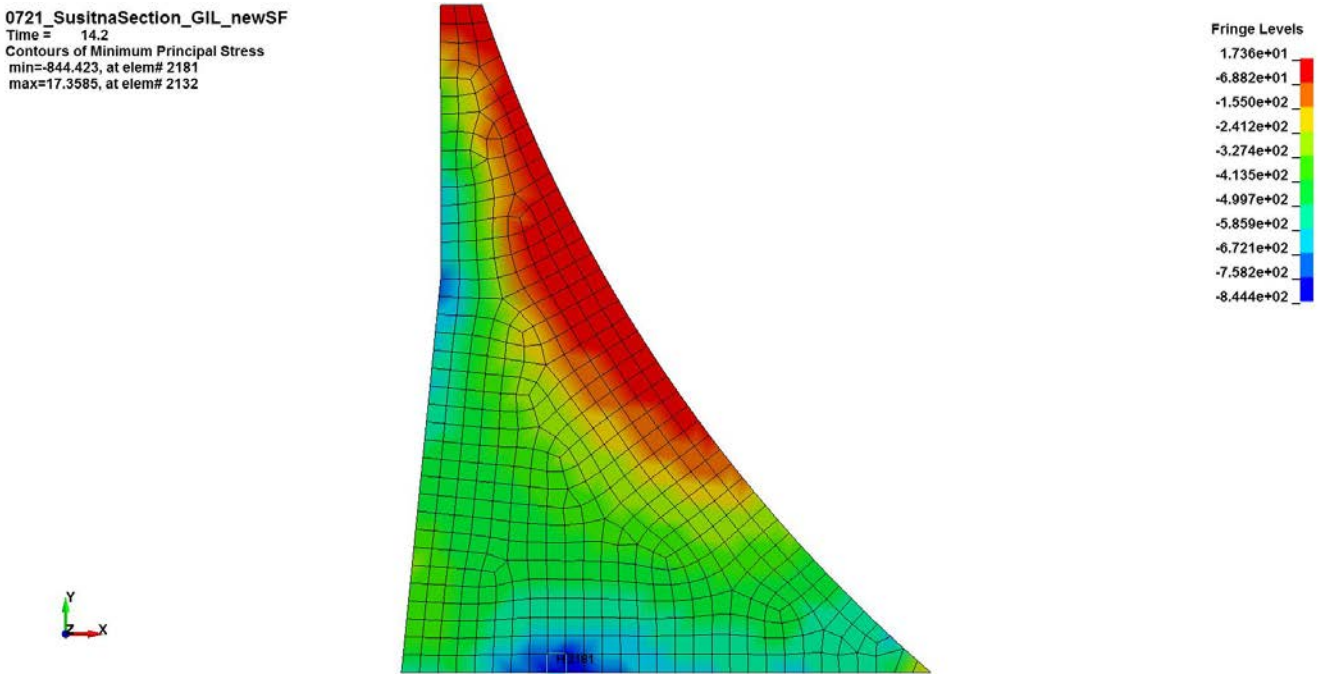

Figure 23 – 3rd Principal Stress at the Moment when it is Minimum on U/S Face of Monolith

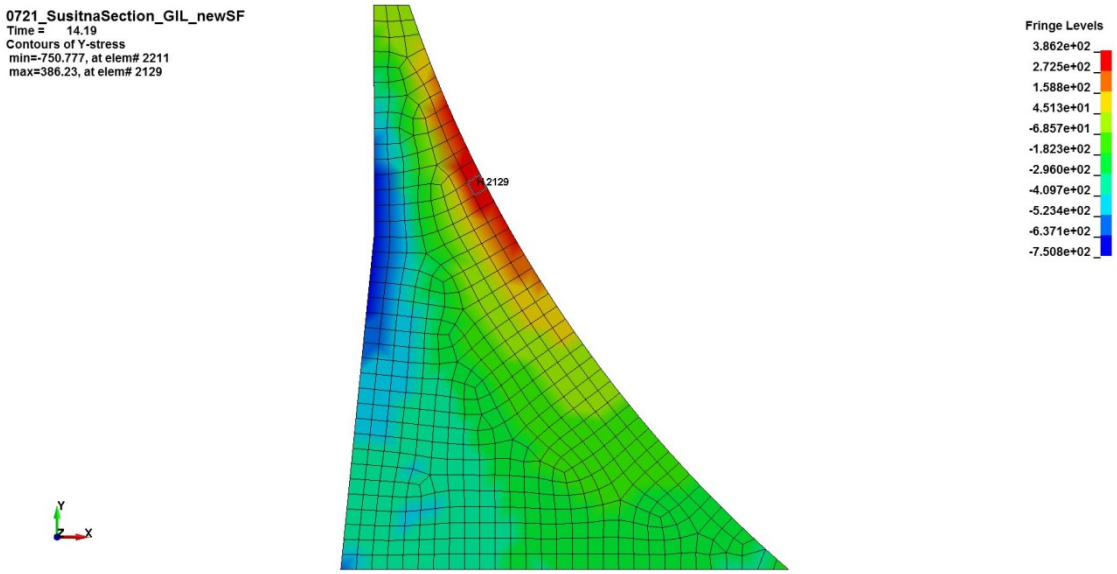

Figure 24 – Vertical Stress at the Moment when it is Maximum on D/S Face of Monolith

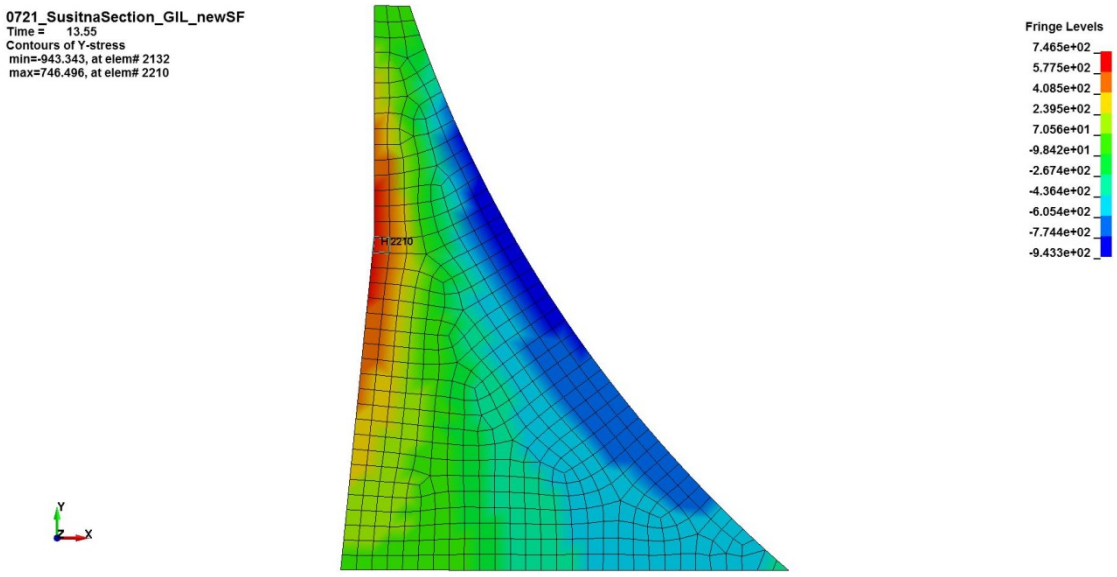

Figure 25 – Vertical Stress at the Moment when it is Maximum on U/S Face of Monolith

11.3. Comparative Diagrams

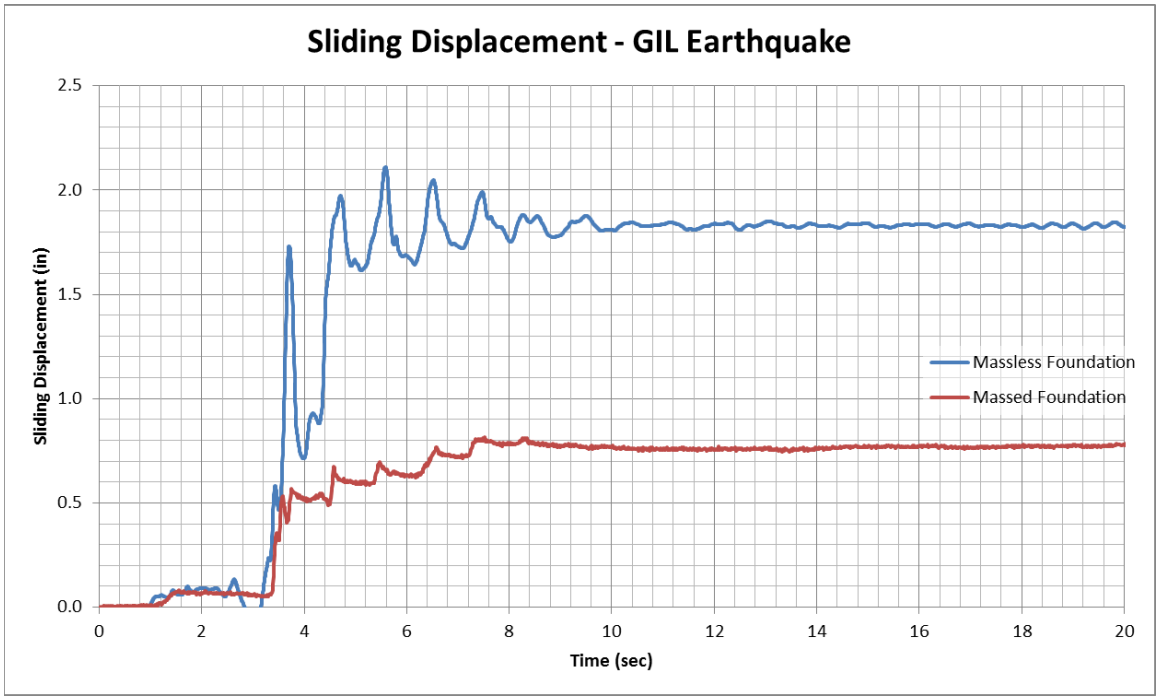

Figure 26 – Sliding Displacement of Dam Monolith

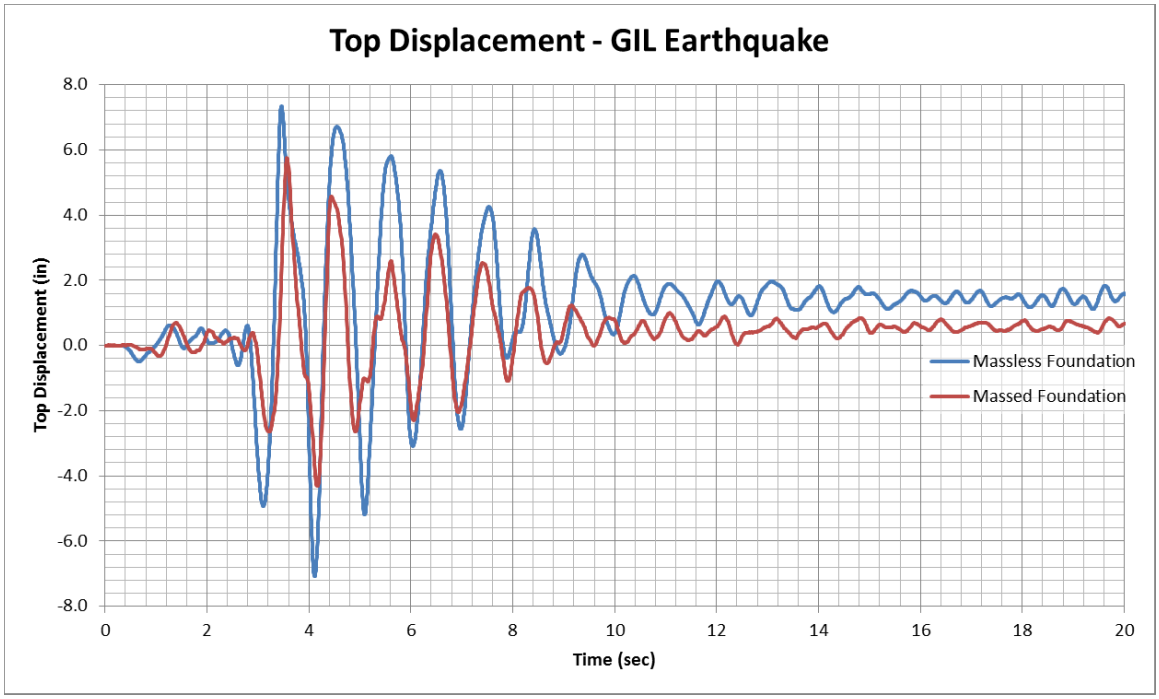

Figure 27 – Top Displacement of Dam Monolith

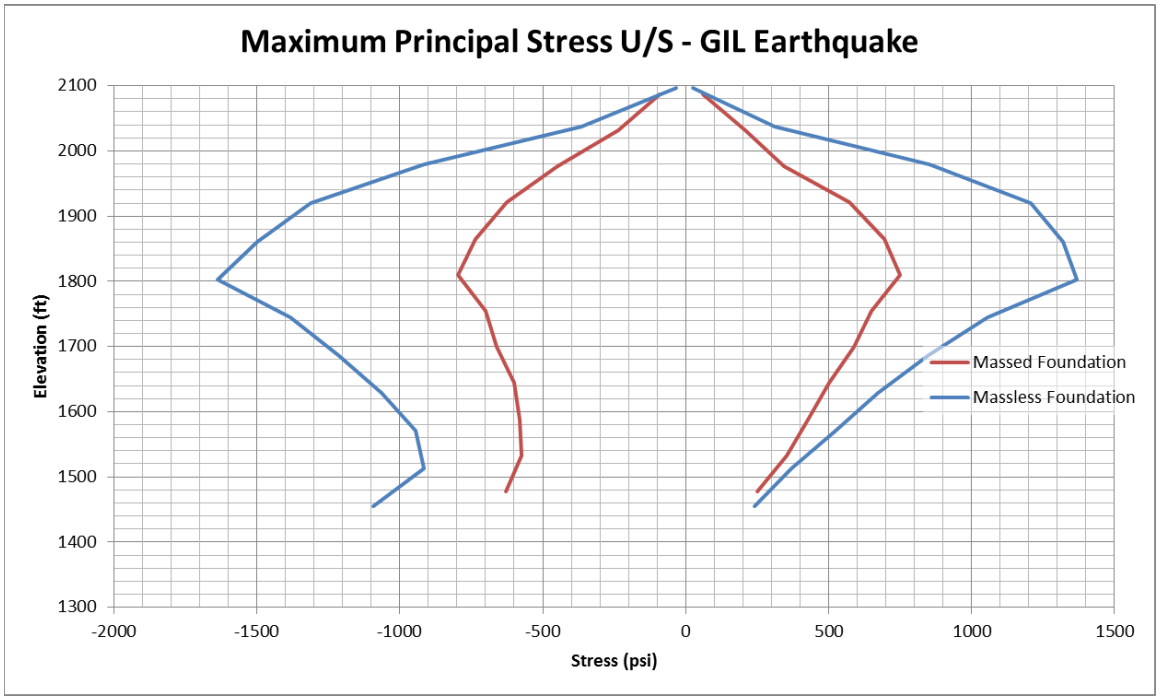

Figure 28 – Maximum Principal Stress on Upstream Face of Dam

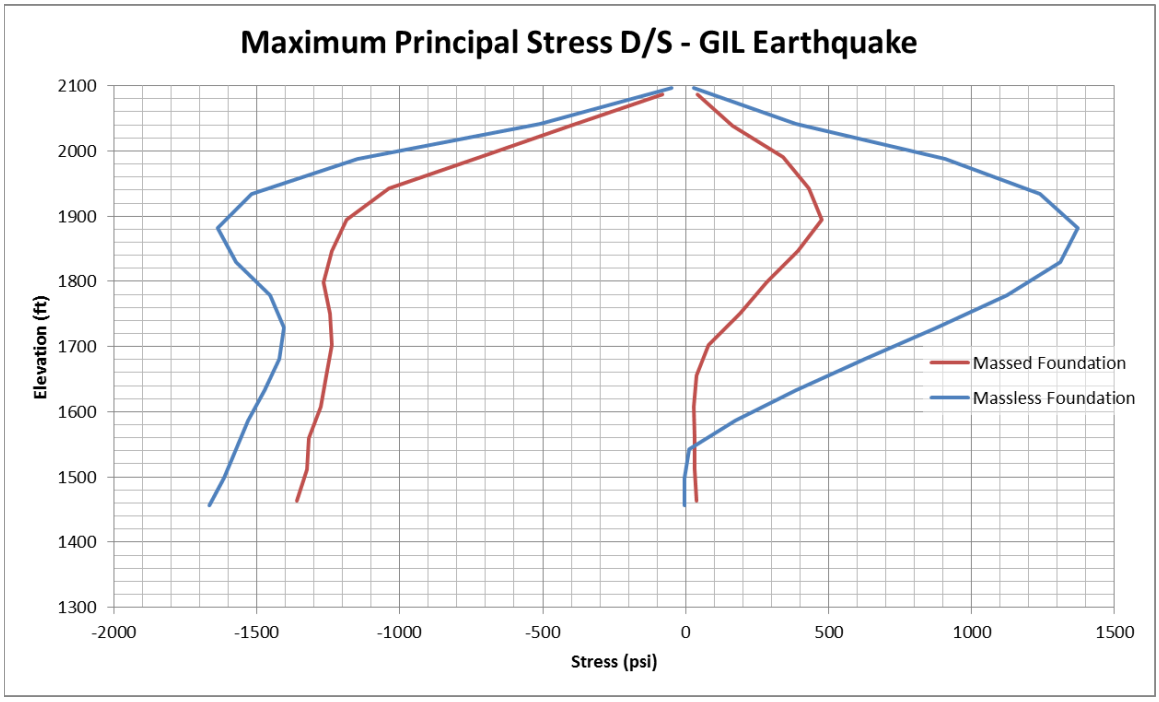

Figure 29 – Maximum Principal Stress on Downstream Face of am

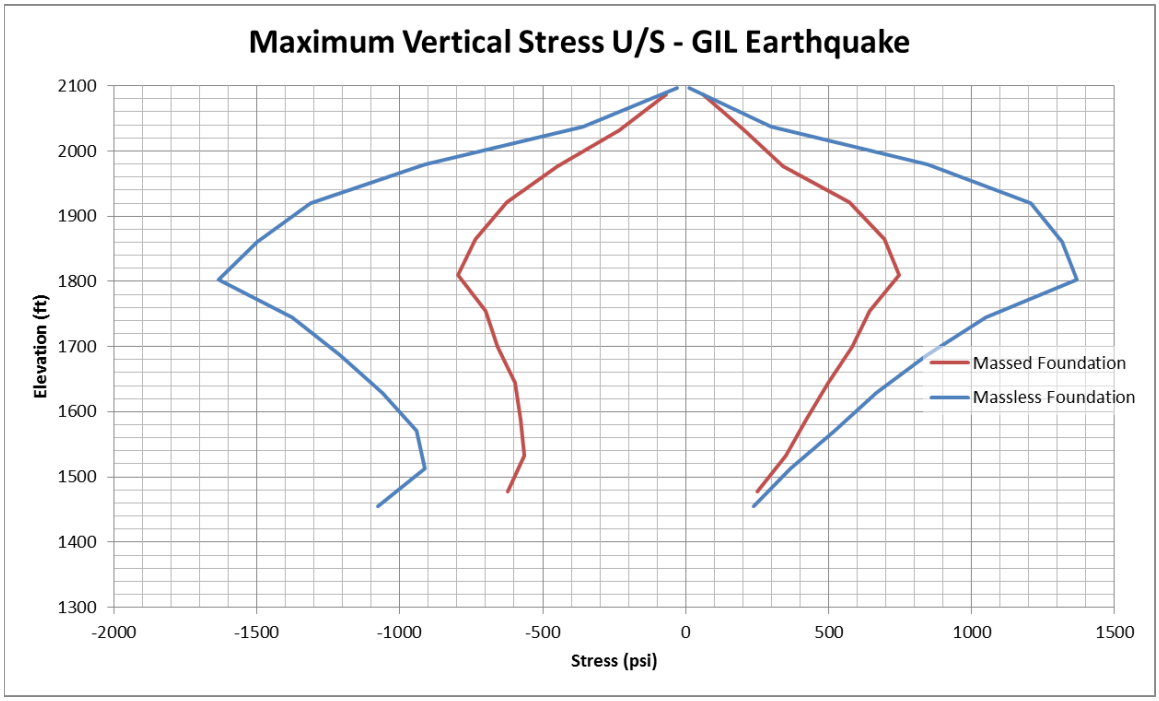

Figure 30 – Maximum Vertical Stress on Upstream Face of Dam

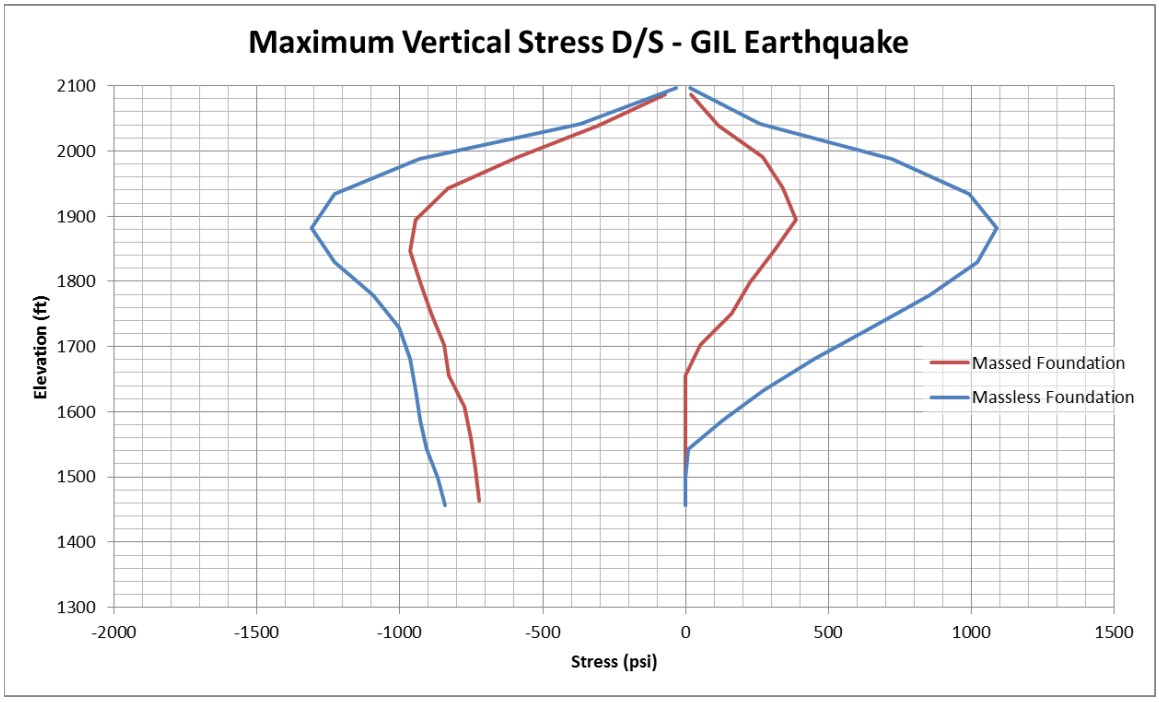

Figure 31 – Maximum Vertical Stress on Downstream Face of Dam

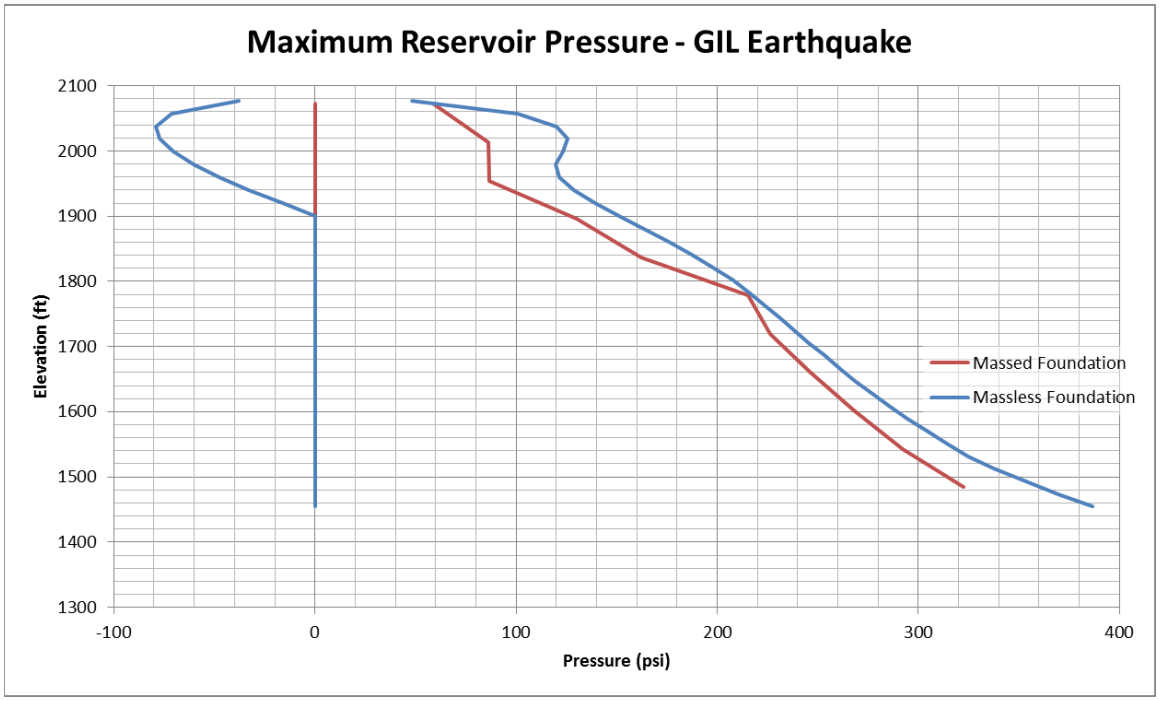

Figure 32 – Maximum Reservoir Pressure at its Interface with Dam

The maximum normal and principal stresses calculated by the two models are listed in Table 11. The table also shows the change in calculated stresses from the inclusion of a massed foundation.

Table 11 – Summary of Maximum Stresses

Model	Location	Principal Stress (psi)		Normal Stress (psi)	
		Tensile	Compressive	Tensile	Compressive
Implicit (Massless)	Upstream	1368	-1635	1366	-1633
	Downstream	1371	-1893	1086	-1309
Explicit (Massed)	Upstream	750	-796	746	-795
	Downstream	477	-1267	386	-964
Change (%)	Upstream	45%	51%	45%	51%
	Downstream	65%	33%	64%	26%

12. Summary

The results presented in this document show that including foundation mass and compressibility of reservoir in the analysis reduces the conservatism of the solution. The seismic demand both in terms of sliding displacement and maximum stress in concrete is also reduced. Table 11 shows that the maximum tensile stresses within the dam body are between 45% and 65% lower in the explicit model.

The analysis described in this report is based on a simple 2D model, but it is recognized that the curved configuration of the dam axis will result in lateral distribution of loads. It is recommended a complete 3D model of the dam-foundation-reservoir should be produced and the results used for design decisions.

13. References

[1] Lysmer, J., et al., “Finite Dynamic Model for Infinite Media,” J. Eng. Mech. Div. ASCE, 589-877, 1969

[2] Joyner, W.B., Chen, A.T.F., “Calculation of Nonlinear Ground Response in Earthquakes,” Bulletin of the Seismological Society of America. Vol. 65, No. 5, pp. 1315-1336, 1975

[3] Mejia, L.H., Dawson, E.M., "Earthquake deconvolution for FLAC," 4th International FLAC Symposium on Numerical Modeling in Geomechanics, 2006

[4] Zienkiewicz, O.C., N. Bicanic and F.Q. Shen, “Earthquake input definition and the transmitting boundary conditions,” Proceedings Advances in Computational Nonlinear Mechanics I, pp. 109-138, Springer-Verlag, 1989

[5] Chopra, A.K., "Earthquake Analysis of Arch Dams: Factors to be Considered," The 14th World Conference on Earthquake Engineering, 2008

[6] Ghanaat, Y., “Theoretical Manual for Analysis of Arch Dams,” USACE ITL, 1993

[7] Ghanaat, Y., Hashimoto, P.S., Zuchuat, O., and Kennedy, R.P., “Seismic fragility of Mühleberg Dam using nonlinear analysis with Latin Hypercube Simulation,” Proceedings of the 31st Annual USSD Conference, San Diego, California, April 11-15, 2011

[8] Alaska Energy Authority, “Meeting No. 4 - Susitna-Watana Dam Project Independent Board of Consultants and Advisors,” Bellevue, WA, April 2 - 4, 2014

[9] Hall, J. F., “Problems Encountered from the Use or Misuse of Rayleigh Damping,” 2006

[10] Westergaard, H.M., “Water pressures on dams during earthquakes,” Transactions of ASCE 98, 418-433, 1931

[11] FERC, “Engineering guideline for the evaluation of hydropower projects,” chapter 11, 1999

[12] Ansys Release 15.0 User Manual, ANSYS Inc., 2013

[13] LS-DYNA Keyword User's Manual, Livermore Software Technology Corporation, 2014